

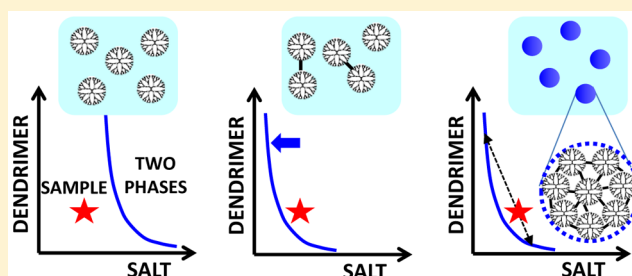
Formation of Dendrimer Nanoassemblies by Oligomerization-Induced Liquid–Liquid Phase Separation

Viviana C. P. da Costa and Onofrio Annunziata*[✉]

Department of Chemistry & Biochemistry, Texas Christian University, Fort Worth, Texas 76129, United States

Supporting Information

ABSTRACT: Dendrimers are hyperbranched macromolecules with applications in host–guest chemistry, self-assembly, nanocatalysis, and nanomedicine. We show that dendrimer-based globular nanoparticles are formed by using dendrimer oligomerization to isothermally induce liquid–liquid phase separation (LLPS). We first determined that LLPS of aqueous mixtures of the fourth-generation amino-functionalized poly-(amido amine) dendrimer is observed by lowering temperature in the presence of sodium sulfate. In relation to LLPS, we experimentally characterized the effect of salt and dendrimer concentrations on the LLPS temperature and salt–dendrimer isothermal partitioning. Our results were theoretically examined using a two-parameter thermodynamic model. We then showed that the addition of a small amount of glutaraldehyde, which leads to the formation of soluble dendrimer oligomers by chemical cross-linking, increases the LLPS temperature. This implies that a dendrimer aqueous mixture, which is initially homogeneous at room temperature and exhibits LLPS only at relatively low temperatures, can exhibit LLPS at room temperature due to dendrimer oligomerization. The high dendrimer concentration inside the nanodroplets, produced from LLPS, accelerates dendrimer cross-linking, thereby yielding stable globular nanoparticles. These nanomaterials retain the host–guest properties of the initial dendrimers, indicating potential applications as nanocatalysts, extracting agents and drug carriers. Our work provides the basis for a new approach for obtaining dendrimer-based nanoassemblies by employing low-generation dendrimers as building blocks.



1. INTRODUCTION

Dendrimers are hyperbranched globular macromolecules that consist of a multifunctional central core to which branching units are sequentially added, resulting in a tree-like structure.^{1–4} The number of branching points, when going radially from the core toward the surface, defines the dendrimer generation (G). Dendrimers possess a large number of terminal groups on their outer shell. These surface groups can be readily modified into a high number and variety of functional groups, which can be used to tune the solubility of these macromolecules in a given solvent. The dendrimer's treelike structure gives rise to the formation of internal cavities, responsible for host–guest interactions.^{5,6} These molecular properties are very important for applications of dendrimers in catalysis, nanotechnology and medicinal chemistry.^{7–10}

High- G dendrimers have the advantage of potentially hosting a relatively high number of guest molecules per macromolecule. However, since the surface density of terminal groups also increases with generation, dendrimers with $G \geq 7$ are more difficult to synthesize¹¹ due to steric hindrance. This also promotes a pronounced backfolding of terminal groups, which causes an increase in conformational rigidity and a decrease of cavity volume per dendrimer mass.^{4,12} Hence, the loading capacity of guest molecules per dendrimer mass is appreciably reduced.^{6,13} These limitations favor the employment of low- G

dendrimers ($4 \leq G \leq 6$) for host–guest applications. Furthermore, the relatively higher flexibility of low- G dendrimers can lead to significant conformational changes due to external stimuli.^{14,15} This aspect is advantageous for applications such as environment-sensitive host–guest binding and chemical sensing. Thus, it is important to identify approaches that would circumvent the need of synthesizing high- G dendrimers and will lead to the preparation of dendrimer materials that retain the high-load capacity of high- G dendrimers and the advantages of low- G dendrimers. One approach is the preparation of nanoassemblies of low- G dendrimers, which may be denoted as megamers.¹⁶ This approach was previously employed to prepare core–shell tecto(dendrimers),^{16–18} where one dendrimer (core) is covalently attached to several relatively smaller dendrimers through their surface functional groups. In this paper, we examine a distinct approach for the preparation of dendrimer nanoassemblies. Specifically, we investigate the use of liquid–liquid phase separation (LLPS)^{19,20} as a means to induce the self-assembly of low- G dendrimers.

Received: March 16, 2017

Revised: April 26, 2017

Published: May 1, 2017

The LLPS of mixtures containing globular macromolecules has been employed for the formation of cross-linked microspheres. In related experiments, a precipitating agent is typically added to the macromolecular solution to induce the formation of macromolecule-rich spherical droplets, a process usually denoted as coacervation or condensation. A chemical cross-linker is then added to the resulting suspension in order to irreversibly produce microspheres. However, this approach yields, in general, relatively large particles, with radii of the order of 10 μm .^{21–23}

For proteins, it has been shown that another approach to obtain protein coacervates is based on oligomerization-induced LLPS.²⁴ Specifically, we consider a protein aqueous solution that is thermodynamically stable at a working temperature (e.g., 20 °C) but undergoes LLPS at a lower temperature (e.g., 0 °C). A small amount of glutaraldehyde, a bifunctional agent that mainly reacts with primary amino groups on the protein surface,²⁵ is then added to the protein solution at the working temperature in order to produce protein soluble oligomers. This isothermal oligomerization process reduces solution mixing entropy thereby raising the LLPS temperature. When the LLPS temperature exceeds the operational temperature, protein condensation into spherical droplets isothermally occurs. The high protein concentration inside the droplets enhances protein cross-linking making the condensation process effectively irreversible.²⁴

Interestingly, related kinetic experiments revealed that the radius of the cross-linked protein droplets becomes smaller when the rate of protein oligomerization is increased.²⁴ This finding can be explained using classical nucleation theory.²⁶ Specifically, a higher oligomerization rate corresponds to a faster increase in LLPS temperature and allows to nucleate protein condensation after a higher LLPS temperature is achieved. This corresponds to a higher supersaturation and, consequently, to a smaller radius of the emerging condensed phase. Based on this mechanism, macromolecules that possess a large number of surface groups prone to cross-linking are predicted to undergo relatively high oligomerization rates. Thus, dendrimers become an ideal candidate for investigating oligomerization-induced LLPS, leading to the formation of particles with radii that are significantly smaller than those typically obtained through traditional coacervation-based methods.

It has been recently shown that LLPS of aqueous solutions of the hydroxyl-functionalized poly(amido amine) dendrimer of fourth generation (G4 PAMAM-OH) can be induced in the presence of strong salting-out agents such as sodium sulfate.²⁷ However, no LLPS study is reported on the corresponding amino-functionalized dendrimer (G4 PAMAM-NH₂), an ideal candidate for glutaraldehyde cross-linking.²⁵ Thus, in this paper, we first show that LLPS can be induced for the G4 PAMAM-NH₂ dendrimer in the presence of aqueous sodium sulfate and then that oligomerization-induced dendrimer condensation yields dendrimer globular nanoparticles.

2. EXPERIMENTAL SECTION

2.1. Materials. Amino-functionalized poly(amido amine) dendrimers of fourth generation were purchased from Dendritech, Inc. (Midland) in a methanol solution. Methanol was removed by drying dendrimer samples in a vacuum oven at 50 °C. The dried samples were then dissolved into water and the drying procedure is repeated to remove residual amounts of methanol. Deionized water was passed through a four-stage Millipore filter system to provide high-purity

water for all the experiments. Dendrimer-water stock solutions were then prepared by weight. The dendrimer molecular weight used to calculate molar concentrations was 14.3 kg·mol⁻¹. Sodium sulfate was purchased from J.T. Baker (Phillipsburg, NJ). A salt-water stock solution of 1 L was prepared and its composition (18.31% w/w) was determined from density measurements on properly diluted solutions using a digital density meter (Mettler/Par, DMA40), thermostated at 25.00 ± 0.01 °C. Density values were converted into the corresponding concentrations using the known²⁸ relation between density and salt composition. Copper sulfate and *N,N*-dimethylindoline dye (phenol blue) were purchased from Sigma-Aldrich (St. Louis, MO). Sodium chloride, glutaraldehyde (25% w/w aqueous solution), toluene, triethanolamine, and silicone oil were purchased from Fisher Scientific (Hampton, NH).

2.2. Measurements of LLPS Temperature. The LLPS temperature, T_{ph} , was determined by measuring the turbidity of ternary dendrimer-salt-water samples as a function of temperature (cloud-point method). Methods and related instrumentation are described in ref 27. A ternary homogeneous small sample ($\approx 100 \mu\text{L}$) with a given composition was prepared by mixing known amounts of water, dendrimer and salt stock solutions. The known weight fractions of dendrimer and salt in the ternary mixture were then converted into dendrimer volume fraction, ϕ_{D} , and salt molar concentration, C_{S} , after estimating the sample density using the known volumetric properties of binary sodium sulfate-water solutions and the dendrimer specific volume of 0.817 g cm⁻³ (see Supporting Information: S1).²⁹ All samples for turbidity measurements were allowed to equilibrate for 2 days at a temperature at which they were homogeneous.

2.3. Measurements of Salt-Dendrimer Partitioning at 25 °C. Salt-dendrimer partitioning measurements were performed as described in ref 27 and references therein. The composition of the two coexisting phases, ($\phi_{\text{D}}^{(\text{I})}$, $C_{\text{S}}^{(\text{I})}$) and ($\phi_{\text{D}}^{(\text{II})}$, $C_{\text{S}}^{(\text{II})}$), was characterized using a spectrophotometric assay based on copper binding (for dendrimer) and a potentiometric assay (for salt).

2.4. Dendrimer Cross-Linking Experiments. Glutaraldehyde-water stock solutions (0.1–5% w/w) were prepared by weight. For a given cross-linking experiment, an initial solution of $\approx 100 \mu\text{L}$ was first prepared by mixing known amounts of water, dendrimer and salt stock solutions at room temperature. A small aliquot of glutaraldehyde stock solution was then added to the dendrimer-salt-water solutions under stirring conditions. LLPS temperatures were determined as described in section 2.2.

2.5. Dynamic Light Scattering. Measurements of dynamic light scattering (DLS) were performed at 25.0 ± 0.1 °C. After glutaraldehyde was added, all dendrimer aqueous samples were promptly filtered through a 0.45 μm filter (Anotop 10, Whatman) and placed in a test tube. The experiments were performed on a light scattering apparatus built using the following main components: He-Ne laser (35 mW, 632.8 nm, Coherent Radiation), manual goniometer and thermostat (Photocor Instruments), multitaу correlator, APD detector, and software (PD4042, Precision Detectors). All measurements were performed at a scattering angle of 90°. The scattering vector $Q = (4\pi n/\lambda)\sin(\theta/2)$ was calculated using $n = 1.33$ and $\lambda = 632.8$ nm. The scattered-intensity correlation functions were analyzed using a regularization algorithm (Precision Deconvolve 32, Precision Detectors). The application of regularization to the experimental correlation function is described in ref 24 and references therein. For monomodal distributions, the observed light-scattering peak is associated with dendrimer oligomers. The corresponding apparent hydrodynamic radius was calculated using the Stokes–Einstein equation: $R_{\text{h}} = k_{\text{B}}T/(6\pi\eta\langle D \rangle_z)$,³⁰ where k_{B} is the Boltzmann constant, T is the absolute temperature, η is the viscosity of the corresponding salt-water solution, and $\langle D \rangle_z$ is the z -average diffusion coefficient. For bimodal distributions, the two light-scattering peaks are associated with dendrimer oligomers (fast diffusion mode) and dendrimer nanoparticles (slow diffusion mode), respectively. The corresponding hydrodynamic radii were calculated from the z -average diffusion coefficient associated with the fast and slow diffusion modes, respectively.

2.6. Scanning Electron Microscopy. Samples containing cross-linked dendrimers were first characterized by DLS and then by field-emission scanning electron microscopy (SEM). Prior to SEM characterization, samples were diluted and dialyzed against water to remove salt ions. Specifically, a given sample ($\approx 100 \mu\text{L}$) was first diluted into 1 mL of water and then dialyzed against water using an ultrafiltration centrifugal device (AmiconUltra, 30 kDa membrane cutoff, Millipore). The final retentate volume was set to $\approx 100 \mu\text{L}$. A small aliquot ($\approx 10 \mu\text{L}$) of the retentate was directly placed on the specimen stub and left to dry overnight under vacuum. After drying, a sample were coated with a 10 nm layer of 60/40 gold/palladium by low-vacuum sputter coating and analyzed with a JSM-7800F field-emission scanning electron microscope (JEOL).

2.7. Phenol Blue Binding Experiments. An aqueous stock solutions of phenol blue (11 μM) was prepared by mixing a known weight of this dye with water in a 1 L volumetric flask. A dendrimer-water stock solution (1.9% w/w, 1.3 mM, 1 mL) was also prepared by weight and mixed with an equal volume of phenol blue stock solution so that the dendrimer molar concentration was 0.65 mM. The molar ratio of dye to dendrimer in the resulting mixture of 2 mL was ≈ 0.01 . This mixture was stirred at room temperature in the dark during the incubation time of 48 h. The absorbance spectrum of the mixture was recorded (DU800, Beckman Coulter) before and after the incubation time. The binding of blue phenol to dendrimer is verified by the occurrence of the wavelength shift of the maximum absorbance from 635 to 545 nm.³¹ Control measurements, directly performed on the phenol blue stock solution before and after the incubation time (also stored in the dark), show no detectable change in the absorption spectrum. After the sample incubation time, toluene (2 mL) was added to the dendrimer-dye aqueous solution. The biphasic sample was thoroughly shaken for 10 min. The sample was then allowed to achieve macroscopic phase separation first by gravity and then by centrifugation (10 min at 2500 rpm, Allegra 25 R centrifuge, Beckman Coulter) until a clear interface is observed between the organic (top) and the aqueous (bottom) phases. Aliquots from both organic and aqueous phases were transferred into different vials and the visible spectrum of each phase was recorded. No phenol blue could be detected in the organic phase by spectrophotometry. In a control experiment, a 2 mL solution of phenol blue, which was prepared by mixing 1 mL of the stock solution with water, was added to an equal volumetric amount of toluene. After the equilibration procedure, the dye transferred to the organic phase and no phenol blue could be detected in the aqueous phase by spectrophotometry. The dye-loaded dendrimer aqueous solution was then cross-linked using glutaraldehyde in the presence of sodium sulfate. Specifically, a 1 mL aliquot of the dye-loaded dendrimer solution was first concentrated by evaporation in a vacuum oven at room temperature and then mixed with a sodium sulfate stock solution and water so that the final sample volume remained of 1 mL. A small amount (60 μL) of aqueous stock solution of glutaraldehyde (5% w/w) was then steadily added to ensure that dendrimer cross-linking and aggregation occurred. The equilibration procedure in the presence of 1 mL of toluene was repeated. After the equilibration procedure, no phenol blue could be detected in the organic phase by spectrophotometry.

3. RESULTS AND DISCUSSION

This section is divided in the following way. First, our experimental results on the LLPS of dendrimer-salt-water mixtures will be reported together with a theoretical analysis of this phase transition based on a two-parameter thermodynamic model. Second, our experimental results describing the effect of dendrimer cross-linking on LLPS, dendrimer oligomerization and the formation of globular dendrimer nanoparticles will be shown. Finally, it is verified that these cross-linked dendrimer materials retain the guest-encapsulation properties of individual dendrimers.

3.1. LLPS of Dendrimer–Salt–Water Mixtures. We explored the effect of salting-out salts on the phase behavior of

aqueous solutions of G4 PAMAM-NH₂. While no phase separation is observed in the presence of sodium chloride, we find that LLPS can be induced by lowering temperature in the presence of sodium sulfate, a stronger salting-out agent according to the Hofmeister series.^{32,33}

In presenting our experimental results, the composition of the investigated ternary dendrimer-salt-water system will be described by the dendrimer volume fraction, ϕ_D , and salt molar concentration, C_S . A given LLPS boundary is described by the LLPS temperature, T_{ph} , as a function of C_S and ϕ_D . At constant temperature, the isothermal phase boundary (C_S , ϕ_D) is denoted as binodal.²⁷ We have experimentally characterized T_{ph} as a function of C_S at several values of ϕ_D . Our results are shown in Figure 1A. In all cases, T_{ph} significantly increases with

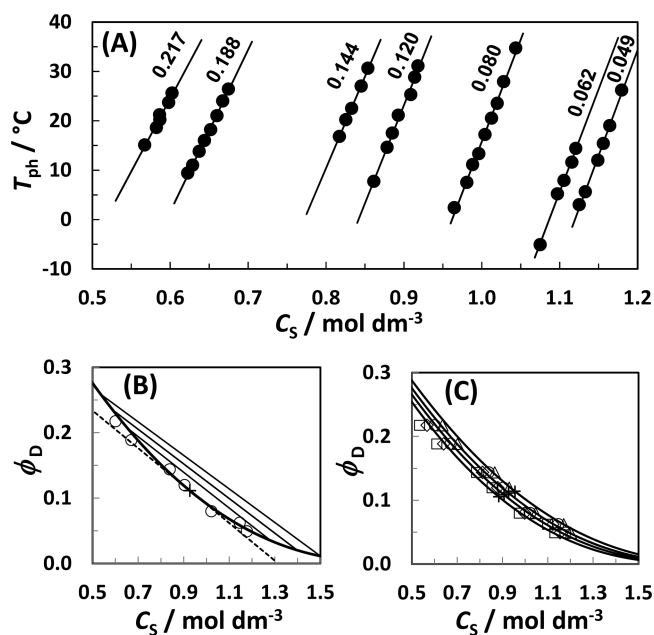


Figure 1. (A) LLPS temperature, T_{ph} , as a function of salt concentration, C_S , at constant dendrimer volume fraction, ϕ_D . The numbers associated with each curve identify the corresponding value of ϕ_D . The solid lines are linear fits through the experimental data. (B) Binodal data, ϕ_D , as a function of C_S , for the dendrimer–salt–water system at 25 °C (circles). The solid curve is the theoretical binodal obtained from the thermodynamic model discussed at the end of this section (see eqs 1–4) with $\epsilon/RT = 25$ ($\epsilon = 62 \text{ kJ}\cdot\text{mol}^{-1}$) and $q = 0.415$. The three solid lines are calculated representative tie-lines. The cross represents the location of the critical point. The dashed line crossing the critical point describes the experimental slope at the critical point. (C) Binodal data, ϕ_D , as a function of C_S , for the dendrimer–salt–water system at four representative temperatures (5 °C, squares; 15 °C, diamonds; 25 °C, circles; 35 °C, triangles). Moving from left to right, the four solid curves are theoretical binodal curves calculated by setting $q = 0.4375$ (5 °C), 0.4250 (15 °C), 0.4150 (25 °C), and 0.4050 (35 °C), respectively. The four crosses represent the location of the critical points.

salt concentration. Specifically, an increment of $\approx 0.05 \text{ mol}\cdot\text{dm}^{-3}$ in salt concentration produces a corresponding increment of $\approx 20 \text{ }^\circ\text{C}$ in the LLPS temperature.

In Figure 1B, we plot our experimental binodal $\phi_D(C_S)$ at $T_{ph} = 25 \text{ }^\circ\text{C}$. This curve, which was obtained by fitting our $T_{ph}(C_S)$ data in Figure 1A at any given ϕ_D to a linear equation, shows that an increment of $\approx 0.1 \text{ mol}\cdot\text{dm}^{-3}$ in salt concentration

reduces the equilibrium dendrimer volume fraction by ≈ 0.03 within the experimental salt concentration range.

At a fixed temperature, LLPS yields the formation of two coexisting liquid phases with compositions ($C_S^{(I)}$, $\phi_D^{(I)}$) and ($C_S^{(II)}$, $\phi_D^{(II)}$) for phases I and II, respectively. We have experimentally characterized these compositions at 25 °C. Our results are reported in Table 1 together with the

Table 1. Salt/Dendrimer Partitioning at 25 °C

$C_S^{(I)}$ (mol dm ⁻³)	$\phi_D^{(I)}$	$C_S^{(II)}$ (mol dm ⁻³)	$\phi_D^{(II)}$	$\Delta C_S/\Delta\phi_D$ (mol dm ⁻³)	q^a
1.23	0.006	0.37	0.34	-2.4	0.29
1.41	0.004	0.39	0.35	-2.7	0.29
1.31	0.010	0.40	0.34	-2.5	0.27
1.61	0.004	0.38	0.38	-3.2	0.31

^aSee eqs 1–4 and related description for the definition of q .

corresponding partition coefficients defined as $\Delta C_S/\Delta\phi_D \equiv (C_S^{(II)} - C_S^{(I)})/(\phi_D^{(II)} - \phi_D^{(I)})$. The negative values of $\Delta C_S/\Delta\phi_D$ reflect the salting-out mechanism: i.e., the preferential hydration^{33,34} of both solute components leads to salt-rich (I) and dendrimer-rich (II) coexisting phases. Note that the reported $\phi_D^{(II)}$ values, which are higher than 0.3, correspond to an average dendrimer–dendrimer distance lower than 4 nm, consistent with the formation of a dendrimer condensed phase in which dendrimer particles with a radius of ≈ 2 nm (see section 3.3) are essentially in contact with each other. In other words, the dendrimer concentration in phase II is comparable with that of crystals and aggregates of colloidal particles.³⁵ On the other hand, dendrimer concentration in the salt-rich phase is significantly lower ($\phi_D^{(I)} \leq 0.01$). These results describe LLPS effectiveness in removing dendrimers from their initial medium.

Our values in Table 1 can be also used to estimate the critical dendrimer volume fraction, $\phi_D^{(c)}$. This was obtained by the linear extrapolation of $(\phi_D^{(I)} + \phi_D^{(II)})/2$ to $|\phi_D^{(I)} + \phi_D^{(II)}|^{1/\beta} \rightarrow 0$, with $\beta = 0.325$ (Ising exponent) and $\beta = 0.5$ (mean-field exponent) (see Supporting Information: S2).³⁶ From the corresponding plots, we found that $\phi_D^{(c)} = 0.12 \pm 0.03$. By fitting the binodal data in Figure 1B to a linear equation, the salt critical concentration of $C_S^{(c)} = (0.9 \pm 0.1)$ mol·dm⁻³ is obtained. We have also extracted the corresponding slope, $(\partial C_S/\partial\phi_D)_T = -(3.45 \pm 0.16)$ mol·dm⁻³. This slope also represents the limiting partition coefficient at the critical point and is comparable with the values of $\Delta C_S/\Delta\phi_D$ in Table 1, which range between -3.2 and -2.4 mol·dm⁻³.

To theoretically describe the observed LLPS boundary, we consider the thermodynamic model introduced in ref 27 and applicable to ternary aqueous solutions of hydrophilic globular particles in the presence of salt at high concentration. This model, which was employed to explain the main features of salt-induced LLPS of aqueous mixtures of G4 PAMAM-OH, is based on the evaluation of an expression for the dendrimer osmotic pressure, $\Pi(\phi_D, C_S, T)$, in a ternary dendrimer–salt–water mixture with composition (ϕ_D, C_S) in equilibrium dialysis with a binary salt–water reservoir with salt concentration $C_S^* = C_S/\alpha$, where $\alpha(\phi_D)$ is the volume fraction of the bulk domain in the ternary system.^{37,38} The bulk domain is a binary salt–water solution with the same composition of the reservoir. Note that the volume fraction, $1 - \alpha$, describes the volume occupied by the dendrimer particles and their adjacent salt-depleted water layer (local domain). Dendrimer particles are assumed to adopt a compact globular state in the presence of

strong salting-out agents due to the reduced solvent quality. Furthermore, the effects of dendrimer charge are neglected due to the relatively high salt ionic strength (higher than 1.5 M; see Figure 1A,B). This second assumption is expected to be more accurate for PAMAM-OH than for PAMAM-NH₂ due to the acid–base properties of the primary amino terminals at our experimental pH values, ranging from 8 (low ϕ_D) to 9 (high ϕ_D). Indeed, titration studies show that the degree of protonation of G4 PAMAM-NH₂ is 30–40% within our experimental pH range. This corresponds to a dendrimer positive charge of 20–25 from the total number of primary amino terminals of 64.³⁹

The dendrimer osmotic pressure, Π , is the difference of a first contribution describing the dendrimer osmotic pressure in the absence of salt, Π_D , and a second contribution directly proportional to salt osmotic pressure, Π_S . The corresponding equation of state is given by²⁷

$$p = p_D - (1 - \alpha + \phi_D\alpha')p_S \quad (1)$$

with

$$p_D = \left(1 + b\phi_D + \frac{e}{RT}\phi_D\right)\phi_D \quad (2)$$

$$\alpha = (1 - \phi_D)\exp[-A\eta_D - B\eta_D^2 - C\eta_D^3 + D\ln(1 + \eta_D)] \quad (3)$$

$$p_S = \gamma_D\nu_S\varphi C_S^*/C_W^* \quad (4)$$

where we have introduced the unitless normalized pressures $p \equiv \Pi V_D/RT$, $p_D \equiv \Pi_D V_D/RT$, and $p_S \equiv \Pi_S V_D/RT$ with V_D , R , and T being dendrimer molar volume, ideal-gas constant, and absolute temperature, respectively. The expression of the reduced chemical potential, μ , is extracted from the integration of the Gibbs–Duhem condition: $(\partial\mu/\partial\phi_D)_{T,p_S} = (\partial p/\partial\phi_D)_{T,p_S}/\phi_D$. In eq 2, we have used $b = (4 - 2\phi_D)/(1 - \phi_D)^3$ based on the Carnahan–Starling equation of state⁴⁰ and $e = (\varepsilon/8)(b + b'\phi_D)\phi_D$, where $b' \equiv db/d\phi_D$ and ε is an energy parameter that is positive for hydrophilic macromolecules (e.g., dendrimers with polar surface groups). This expression of ε is based on the assumption that the range of water-mediated endothermic dendrimer–dendrimer interactions is infinitely short.^{27,41} In eq 3, we have used the Mansoori–Carnahan–Starling–Leland expression of α ,^{42,43} with $\eta_D \equiv \phi_D/(1 - \phi_D)$, $A \equiv 3q + 6q^2 - q^3$, $B \equiv 3q^2 + 4q^3$, $C \equiv 2q^3$ and $D \equiv 3q^2 - 2q^3$, where q is a positive parameter representing the ratio of the thickness of the salt-depleted water layer to the radius of the dendrimer particle. Note that q characterizes the magnitude of the dendrimer–salt salting-out interactions. In eq 4, $\gamma_D \equiv V_D/V_W = 645$ is the dendrimer-to-water volume ratio, $\nu_S = 3$ is the number of ions in sodium sulfate, $\varphi(C_S^*, T)$ is the known⁴⁴ osmotic coefficient of the binary salt–water system and C_W^* the corresponding water concentration (see Supporting Information: S3).

At given values of T , ε and q , the theoretical binodal is calculated by numerically determining the pairs of values $(\phi_D^{(I)}, \phi_D^{(II)})$ that satisfy the equilibrium conditions: $p(\phi_D^{(I)}) = p(\phi_D^{(II)})$ and $\mu(\phi_D^{(I)}) = \mu(\phi_D^{(II)})$ for a set of corresponding values of p_S . The linked pairs of salt concentrations, $(C_S^{(I)}, C_S^{(II)})$, are obtained by first extracting C_S^* from eq 4 and then applying $C_S^{(I)} = C_S^*\alpha(\phi_D^{(I)})$ and $C_S^{(II)} = C_S^*\alpha(\phi_D^{(II)})$. The compositions of the two coexisting phases, $(C_S^{(I)}, \phi_D^{(I)})$ and $(C_S^{(II)}, \phi_D^{(II)})$, are connected by tie lines. The critical point is calculated by the

linear extrapolation of $(\phi_D^{(II)} + \phi_D^{(I)})/2$ and p_S to $|\phi_D^{(II)} - \phi_D^{(I)}|^2 \rightarrow 0$, consistent with the mean-field nature of the model.

In Figure 1B, we include the binodal calculated using the values of $q = 0.415$ and $\varepsilon/RT = 25$ ($\varepsilon = 62 \text{ kJ}\cdot\text{mol}^{-1}$). These values were chosen to match both the location of the experimental binodal in the phase diagram and the experimental slope $(\partial C_S/\partial \phi_D)_T$ (see Supporting Information: S2). The calculated value of $\phi_D^{(c)} = 0.111$ is consistent with our partition results within the experimental error. The positive value of ε , which corresponds to endothermic dendrimer-dendrimer interactions, is in qualitative agreement with the exothermic heat-of-dilution results obtained by isothermal titration calorimetry (see details in Supporting Information: S4).²⁷

In Figure 1C, we plot four experimental binodals extracted at the representative temperatures of $T_{ph} = 5, 15, 25,$ and $35 \text{ }^\circ\text{C}$, respectively. As temperature increases, the binodal shifts toward higher salt concentration. In this figure, we have also included theoretical binodal curves extracted from the thermodynamic model. To reproduce the experimental trend, the value of q was decreased as temperature increases while the value of ε was kept constant (see Supporting Information: S2). Thus, the observed thermal behavior of LLPS is explained by an increase of salting-out strength of salt as temperature is lowered.

3.2. Effect of Dendrimer Oligomerization on LLPS Temperature. In the previous section, we have shown that LLPS of a dendrimer aqueous system can be induced in the presence of sodium sulfate. In this section, we examine the effect of dendrimer self-association on this LLPS. The LLPS domain in the phase diagram of solutions of globular particles is expected to expand in the presence of particle self-associative processes. This has been theoretically examined for suspensions of chains of hard spheres.^{45,46} For example, in the presence of chain-chain attractive interactions, the phase separation temperature increases with the number of linked hard spheres at constant particle volume fraction. This effect has been experimentally demonstrated for aqueous solutions of globular proteins undergoing reversible⁴⁷ and irreversible^{24,48} self-association. Finally, recent experimental and theoretical studies showed that multivalent metal ions can also induce LLPS in aqueous solutions of globular proteins. In this case, a multivalent metal ion (yttrium) binds to protein acidic residues, thereby acting as a bridge between neighboring proteins.^{49–51}

To bring about dendrimer self-association, small amounts of glutaraldehyde were added to dendrimer-salt-water mixtures. This bifunctional cross-linker binds to the terminal amino groups of our dendrimer thereby producing dendrimer soluble oligomers, with the oligomer size increasing with cross-linker concentration (see section 3.4). To verify that the cross-linking reaction reaches completion, light-scattering intensity, which is expected to increase with the average degree of oligomerization, was monitored as a function of time. Our light-scattering experiments show that no change in sample light-scattering intensity is observed after 10 min within the experimental error.

To characterize the effect of dendrimer self-association on LLPS, we have measured the LLPS temperature, T_{ph} , as a function of cross-linker concentration, C_{CL} . LLPS measurements performed at 10 and 120 min show no further change in T_{ph} after 10 min within the experimental error. In Figure 2, we show our results for a ternary mixture ($\phi_D = 0.048, C_S = 1.0 \text{ mol}\cdot\text{dm}^{-3}$) that exhibits LLPS at $T_{ph} = -12.0 \text{ }^\circ\text{C}$ in the absence of cross-linker. Specifically, we plot T_{ph} as a function of the molar ratio, C_{CL}/C_D , with $C_D = 4.1 \times 10^{-3} \text{ mol}\cdot\text{dm}^{-3}$ being the

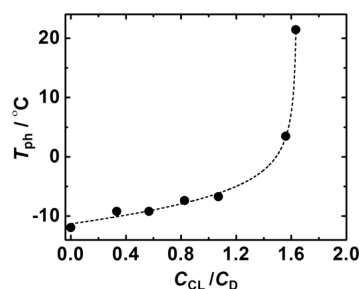


Figure 2. LLPS temperature as a function of cross-linker-to-dendrimer molar ratio, C_{CL}/C_D . Experiments were performed at the constant dendrimer volume fraction of $\phi_D = 0.048$ (molar concentration of $C_D = 4.1 \times 10^{-3} \text{ mol}\cdot\text{dm}^{-3}$) and sodium sulfate molar concentration of $C_S = 1.0 \text{ mol}\cdot\text{dm}^{-3}$. The dashed curve is a guide to the eye.

dendrimer molar concentration. As we can see in this figure, T_{ph} shows a weak dependence on C_{CL}/C_D at low cross-linker concentrations and then sharply increases approaching room temperature after C_{CL}/C_D reaches a value of ≈ 1.5 . This behavior can be related to glutaraldehyde oligomerization in solution.²⁵ Since the concentration of glutaraldehyde oligomers increases with C_{CL} , our results are consistent with a reaction mechanism in which the presence of glutaraldehyde oligomers is necessary for dendrimer cross-linking. The same behavior was observed in the case of protein cross-linking.²⁴

Finally, we remark that the existence of LLPS for the monomeric dendrimer represents a necessary prerequisite for the observation of LLPS in the presence of cross-linker. Indeed, experiments in which sodium chloride replaces sodium sulfate at the same ionic strength ($C_S = 3.0 \text{ mol}\cdot\text{dm}^{-3}$ for NaCl) show that samples remain clear at temperatures as low as $-15 \text{ }^\circ\text{C}$ and C_{CL}/C_D as high as $C_{CL}/C_D = 3$.

3.3. Formation of Dendrimer Globular Nanoparticles.

Our results in section 3.2 indicate that LLPS of dendrimer aqueous solutions may be isothermally induced at room temperature by inducing dendrimer oligomerization in the presence of a small amount of cross-linker. This oligomerization-induced LLPS should manifest itself as the formation of globular condensates.

To experimentally examine this mechanism, dendrimer oligomerization and condensation were investigated by DLS at $25 \text{ }^\circ\text{C}$. Specifically, we have characterized light-scattering particle-size distributions as a function of C_{CL}/C_D at the dendrimer concentration of $C_D = 0.75 \times 10^{-3} \text{ mol}\cdot\text{dm}^{-3}$ ($\phi_D = 0.0087$) and sodium sulfate concentration of $C_S = 0.37 \text{ mol}\cdot\text{dm}^{-3}$. The dendrimer concentration was chosen to be relatively low in order to justify the use of the Stokes–Einstein equation²¹ for the determination of the particle hydrodynamic radius, R_h . At the chosen sodium sulfate concentration, equilibrium DLS distributions could be successfully measured for C_{CL}/C_D ratios as high as 14. At higher values of C_{CL}/C_D , dendrimer cross-linking results in dendrimer macroscopic precipitation. In Figure 3, we show DLS distributions obtained at four representative C_{CL}/C_D ratios. At low C_{CL}/C_D , DLS distributions are monomodal with the average R_h increasing with C_{CL}/C_D starting from the radius of $R_h = 2.0 \text{ nm}$ for the dendrimer monomer (see Figure 3A,B). This behavior characterizes the increase of dendrimer oligomer size with cross-linker concentration. At $C_{CL}/C_D = 10$, the DLS distribution becomes bimodal (see Figure 3C). Specifically, a population of large dendrimer nanoparticles with $R_h \approx 70 \text{ nm}$ separates from the population of dendrimer oligomers with R_h

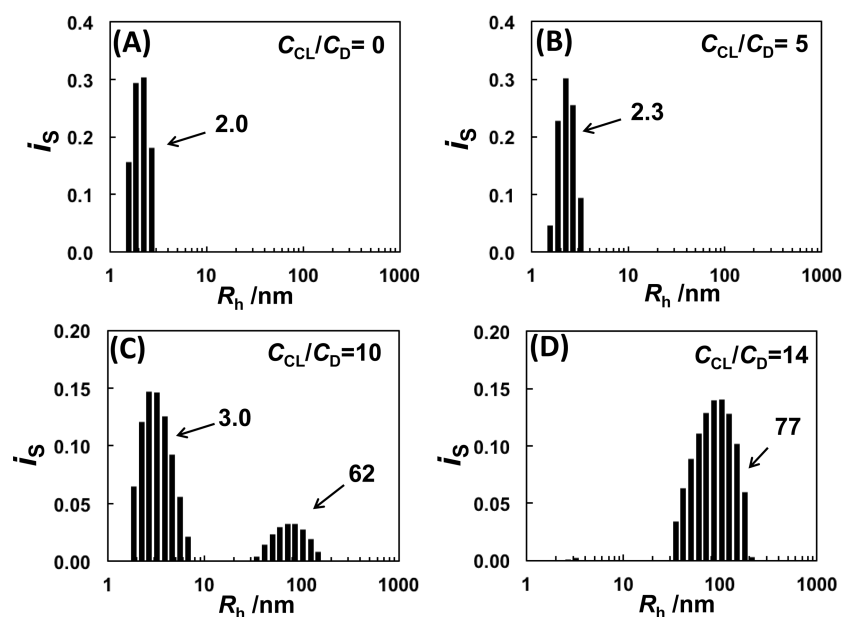


Figure 3. Normalized light-scattering intensity, i_s , as a function of hydrodynamic radius, R_h , at the constant dendrimer volume fraction of $\phi_D = 0.0085$ ($C_D = 0.73 \times 10^{-3} \text{ mol}\cdot\text{dm}^{-3}$), sodium sulfate concentration of $C_S = 0.37 \text{ mol}\cdot\text{dm}^{-3}$, and four representative cross-linker-to-dendrimer molar ratios, C_{CL}/C_D (A–D). The numbers associated with each peak represent the value of R_h/nm calculated from the corresponding z -average diffusion coefficient. Measurements were performed at 25 °C.

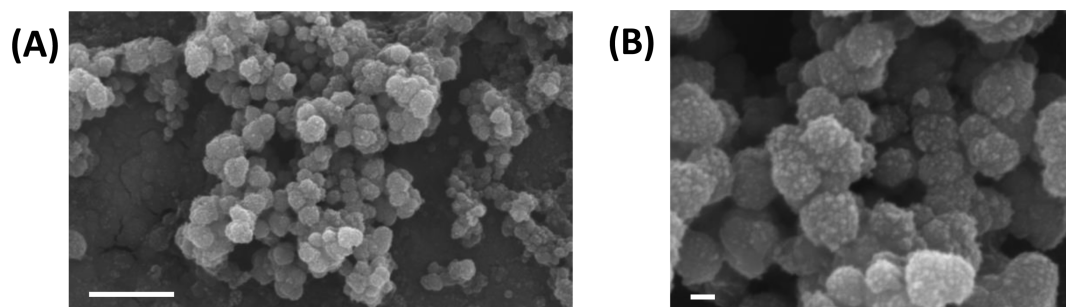


Figure 4. Scanning electron micrographs showing dendrimer nanospheres with a radius of about 100 nm. The horizontal bar represents 1 μm (A) and 100 nm (B).

$\approx 3 \text{ nm}$. As the C_{CL}/C_D ratio further increases, the DLS peak associated with dendrimer nanoparticles becomes dominant (see Figure 3D). The dendrimer nanoparticles represent the formation of a new condensed phase with the value $C_{CL}/C_D = 10$ characterizing the corresponding phase boundary.

The dilution of the samples containing dendrimer nanoparticles and their dialysis against water (to remove salt) established that the formation of these nanoparticles is an irreversible process. This can be understood by realizing that dendrimer–dendrimer cross-linking within these globular condensates is enhanced due to the high dendrimer concentration. SEM images taken after water evaporation show the formation of globular nanoparticles with an average radius of about 100 nm. This is illustrated in Figure 4.

For comparison, DLS experiments were also performed on dendrimer aqueous solutions in the presence of sodium chloride at the same salt ionic strength of sodium sulfate. The obtained particle-size distributions at four representative C_{CL}/C_D ratios ranging from 0 to 19 are shown in Figure 5. All DLS distributions in the presence of NaCl are monomodal with R_h smoothly increasing with C_{CL}/C_D as expected from dendrimer oligomerization. Corresponding SEM images show no formation of globular nanoparticles. At higher values of

C_{CL}/C_D , dendrimer cross-linking results in dendrimer macroscopic precipitation. These results are consistent with NaCl not being able to induce LLPS of dendrimer aqueous solutions.

3.4. Guest Binding Properties. Since polyamidoamine dendrimers can bind small organic molecules, it is important to verify that the investigated dendrimer condensation process does not disrupt dendrimer host–guest properties. This was examined by evaluating the partitioning of a model guest molecule between an aqueous phase containing the host dendrimers and a nonpolar organic phase toward which the guest molecule and the host system exhibit high and poor affinity, respectively. In our case, we chose phenol blue as the guest molecule, a dye that has a relatively high affinity toward toluene compared to water and that is known to bind to PAMAM-NH₂ (in molar excess).³¹ Our results are illustrated in Figure 6. We found that phenol blue quantitatively transfers from the bottom aqueous to the top organic phase in the absence of dendrimer (see Figure 6A). If dendrimers are introduced in the aqueous phase, phenol blue is not detected in the organic phase by spectrophotometry (see Figure 6B). If the guest-loaded dendrimers are cross-linked in the presence of sodium sulfate to achieve dendrimer condensation, blue phenol remains in the aqueous phase (see Figure 6C). This experiment

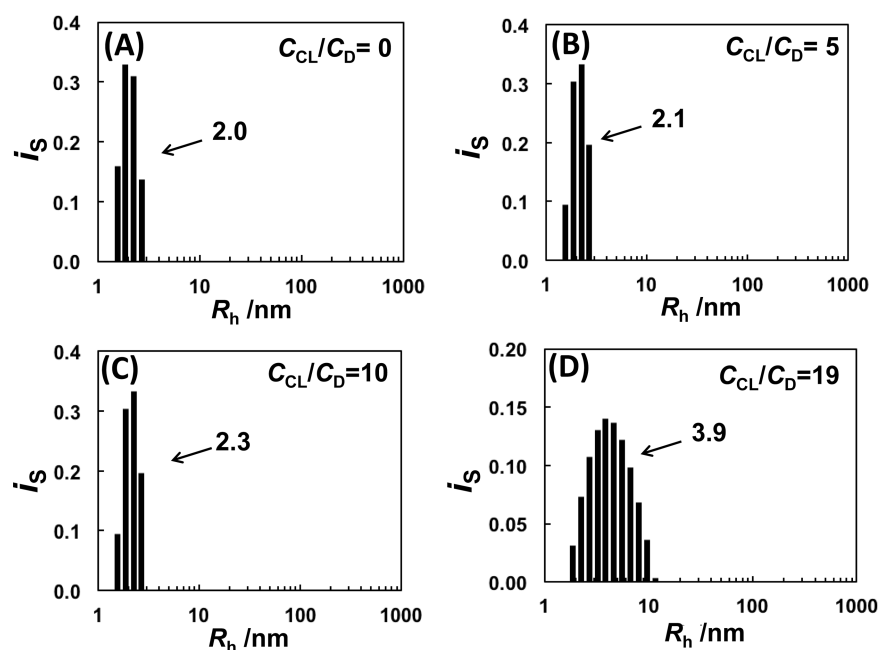


Figure 5. Normalized light-scattering intensity, i_s , as a function of hydrodynamic radius, R_h , at the constant dendrimer volume fraction of $\phi_D = 0.0085$ ($C_D = 0.73 \times 10^{-3} \text{ mol}\cdot\text{dm}^{-3}$), sodium chloride concentration of $C_S = 1.0 \text{ mol}\cdot\text{dm}^{-3}$, and four representative cross-linker-to-dendrimer molar ratios, C_{CL}/C_D (A–D). The numbers associated with each peak represent the value of R_h/nm calculated from the corresponding z -average diffusion coefficient. Measurements were performed at 25°C .

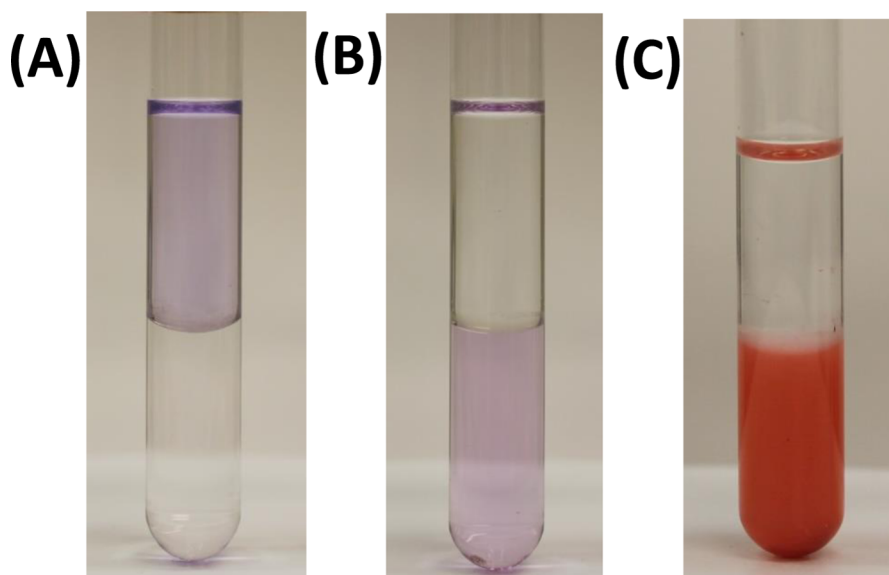


Figure 6. Partition equilibrium of phenol blue between an organic phase (toluene, top) and an aqueous phase (bottom) at room temperature. Phenol blue is initially in the aqueous phase with concentration of $0.5 \times 10^{-6} \text{ mol}\cdot\text{dm}^{-3}$. Phenol blue transfers to the organic phase when the aqueous phase is pure water (A), while it does not transfer to the organic phase when the aqueous phase contains dendrimers (B) with $\phi_D = 0.008$ ($C_D = 0.7 \times 10^{-3} \text{ mol}\cdot\text{dm}^{-3}$), or their cross-linked nanomaterial (C).

shows that dendrimer host–guest properties are retained after dendrimer condensation. Thus, dendrimer nanoparticles can encapsulate guest molecules.

4. SUMMARY AND CONCLUSIONS

We have first showed that LLPS of G4 PAMAM-NH₂ aqueous solutions can be induced in the presence of strong salting-out agents such as Na₂SO₄, while no LLPS is observed in the presence of NaCl, a milder salting-out agents. We have then showed that the coupling of LLPS with dendrimer oligomeriza-

tion induces the irreversible formation of dendrimer globular nanoparticles with radius of $\approx 100 \text{ nm}$. Related experiments in which NaCl replaces Na₂SO₄ establish the key role of LLPS in the observed nanocondensation. This investigation provides the basis for the development of novel dendrimer globular nanoparticles using low generation dendrimers as the building blocks. The approach discussed in this paper can be also extended to systems containing two distinct macromolecules such as dendrimers and proteins. The resulting protein-dendrimer nanomaterials may find applications in catalysis and drug delivery.

■ ASSOCIATED CONTENT

Supporting Information

The Supporting Information is available free of charge on the ACS Publications website at DOI: 10.1021/acs.langmuir.7b00911.

Details on LLPS results, osmotic-coefficient data of binary sodium sulfate-water solutions and heat-of-dilution results on dendrimer aqueous solution (PDF)

■ AUTHOR INFORMATION

Corresponding Author

*Phone: 817-257-6215. Fax: 817-257-5851. E-mail: O. Annunziata@tcu.edu.

ORCID

Onofrio Annunziata: 0000-0002-6636-4750

Notes

The authors declare no competing financial interest.

■ ACKNOWLEDGMENTS

We thank Jeffrey Coffer and Nelli Bodiford for their assistance with SEM experiments. This work was supported by the NSF RI grant (CHE-1126710) and TCU Research and Creative Activity Funds.

■ REFERENCES

- (1) Tomalia, D. A.; Khanna, S. N. A Systematic Framework and Nanoperiodic Concept for Unifying Nanoscience: Hard/Soft Nanoelements, Superatoms, Meta-Atoms, New Emerging Properties, Periodic Property Patterns, and Predictive Mendeleev-like Nanoperiodic Tables. *Chem. Rev.* **2016**, *116*, 2705–2774.
- (2) Tomalia, D. A.; Naylor, A. M.; Goddard, W. A. Starburst Dendrimers: Molecular-Level Control of Size, Shape, Surface Chemistry, Topology, and Flexibility from Atoms to Macroscopic Matter. *Angew. Chem., Int. Ed. Engl.* **1990**, *29*, 138–175.
- (3) Wang, Y.; Salmon, L.; Ruiz, J.; Astruc, D. Metallo-dendrimers in three oxidation states with electronically interacting metals and stabilization of size-selected gold nanoparticles. *Nat. Commun.* **2014**, *5*, 3489.
- (4) Tomalia, D. A.; Christensen, J. B.; Boas, U. *Dendrimers, Dendrons and Dendritic Polymers: Discovery, Applications, the Future*; Cambridge University Press: New York, 2012.
- (5) Jansen, J. F. G. A.; de Brabander-van den Berg, E. M. M.; Meijer, E. W. Encapsulation of Guest Molecules into a Dendritic Box. *Science* **1994**, *266*, 1226–1229.
- (6) Lim, J.; Pavan, G. M.; Annunziata, O.; Simanek, E. Experimental and Computational Evidence for an Inversion in Guest Capacity in High Generation Triazine Dendrimer Hosts. *J. Am. Chem. Soc.* **2012**, *134*, 1942–1945.
- (7) Crooks, R. M.; Zhao, M.; Sun, L.; Chechik, V.; Yeung, L. K. Dendrimer-encapsulated metal nanoparticles: synthesis, characterization, and applications to catalysis. *Acc. Chem. Res.* **2001**, *34*, 181–90.
- (8) Medina, S. H.; El-Sayed, M. E. H. Dendrimers as Carriers for Delivery of Chemotherapeutic Agents. *Chem. Rev.* **2009**, *109*, 3141–3157.
- (9) Caminade, A.-M.; Fruchon, S.; Turrin, C.-O.; et al. The key role of the scaffold on the efficiency of dendrimer nanodrugs. *Nat. Commun.* **2015**, *6*, 7722.
- (10) Mishra, M. K.; Beaty, C. A.; Lesniak, W. G.; et al. Dendrimer Brain Uptake and Targeted Therapy for Brain Injury in a Large Animal Model of Hypothermic Circulatory Arrest. *ACS Nano* **2014**, *8*, 2134–2147.
- (11) Lim, J.; Kostianen, M.; Maly, J.; da Costa, V. C. P.; Annunziata, O.; Pavan, G. M.; Simanek, E. E. Synthesis of large dendrimers with the dimensions of small viruses. *J. Am. Chem. Soc.* **2013**, *135*, 4660–4663.

(12) Maiti, P. K.; Cagin, T.; Wang, G.; Goddard, W. A. Structure of PAMAM Dendrimers: Generations 1 through 11. *Macromolecules* **2004**, *37*, 6236–6254.

(13) Niu, Y.; Yeung, L. K.; Crooks, R. M. Size-Selective Hydrogenation of Olefins by Dendrimer-Encapsulated Palladium Nanoparticles. *J. Am. Chem. Soc.* **2001**, *123*, 6840–6846.

(14) Liu, Y.; Bryantsev, V. S.; Diallo, M. S.; Goddard, W., III. PAMAM dendrimers undergo pH responsive conformational changes without swelling. *J. Am. Chem. Soc.* **2009**, *131*, 2798–2799.

(15) Maiti, P. K.; Çağın, T.; Lin, S.-T.; Goddard, W. Effect of Solvent and pH on the Structure of PAMAM Dendrimers. *Macromolecules* **2005**, *38*, 979–991.

(16) Uppuluri, S.; Swanson, D. R.; Piehler, L. T.; Li, J.; Hagnauer, G. L.; Tomalia, D. A. Core-Shell Tecto(dendrimers). I. Synthesis and Characterization of Saturated Shell Models. *Adv. Mater.* **2000**, *12*, 796–800.

(17) Tomalia, D. A.; Uppuluri, S.; Swanson, D. R.; Li, J. Dendrimers as Reactive Modules for the Synthesis of New Structure Controlled Higher-Complexity Megamers. *Pure Appl. Chem.* **2000**, *72*, 2343–2358.

(18) Tomalia, D. A.; Brothers, H. M., II; Piehler, L. T.; Durst, D. H.; Swanson, D. R. Partial Shell Filled Core-Shell Tecto(dendrimers): A Strategy to Surface Differentiated Nano-Clefts and Cusps. *Proc. Natl. Acad. Sci. U. S. A.* **2002**, *99*, 5081–5087.

(19) Wang, Y.; Lomakin, A.; Latypov, R. F.; Benedek, G. B. Phase separation in solutions of monoclonal antibodies and the effect of human serum albumin. *Proc. Natl. Acad. Sci. U. S. A.* **2011**, *108*, 16606–16611.

(20) Annunziata, O.; Asherie, N.; Lomakin, A.; Pande, J.; Ogun, O.; Benedek, G. B. Effect of polyethylene glycol on the liquid-liquid phase transition in aqueous protein solutions. *Proc. Natl. Acad. Sci. U. S. A.* **2002**, *99*, 14165–14170.

(21) Elbert, D. L. Liquid–liquid two-phase systems for the production of porous hydrogels and hydrogel microspheres for biomedical applications: A tutorial review. *Acta Biomater.* **2011**, *7*, 31–56.

(22) Nichols, M. D.; Scott, E. A.; Elbert, D. L. Factors affecting size and swelling of poly(ethylene glycol) microspheres formed in aqueous sodium sulfate solutions without surfactants. *Biomaterials* **2009**, *30*, 5283–5291.

(23) Lima, A. C.; Sher, P.; Mano, J. F. Production methodologies of polymeric and hydrogel particles for drug delivery applications. *Expert Opin. Drug Delivery* **2012**, *9*, 231–248.

(24) Wang, Y.; Annunziata, O. Liquid-liquid phase transition of protein aqueous solutions isothermally induced by protein cross-linking. *Langmuir* **2008**, *24*, 2799–2807.

(25) Migneault, I.; Dartiguenave, C.; Bertrand, M. J.; Waldron, K. C. Glutaraldehyde: behavior in aqueous solution, reaction with proteins, and application to enzyme crosslinking. *BioTechniques* **2004**, *37*, 370–802.

(26) Kashchiev, D. *Nucleation: basic theory with applications*; Butterworth–Heinemann: Oxford, 2000.

(27) da Costa, V. C. P.; Annunziata, O. Unusual liquid-liquid phase transition in aqueous mixtures of a well-known dendrimer. *Phys. Chem. Chem. Phys.* **2015**, *17*, 28818–28829.

(28) Rard, J. A.; Albright, J. G.; Miller, D. G.; Zeidler, M. E. Ternary mutual diffusion coefficients and densities of the system $\{z_1\text{NaCl} + (1 - z_1)\text{Na}_2\text{SO}_4\}$ (aq) at 298.15 K and a total molarity of 0.5000 mol dm⁻³. *J. Chem. Soc., Faraday Trans.* **1996**, *92*, 4187–4197.

(29) Nourse, A.; Millar, D. B.; Minton, A. P. Physicochemical Characterization of Generation 5 Polyamidoamine Dendrimers. *Biopolymers* **2000**, *53*, 316–328.

(30) Pecora, R. *Dynamic light scattering*; Plenum Press: New York, 1985.

(31) Richter-Egger, D. L.; Landry, J. C.; Tesfai, A.; Tucker, S. A. Spectroscopic Investigations of Polyamido Amine Starburst Dendrimers Using the Solvatochromic Probe Phenol Blue. *J. Phys. Chem. A* **2001**, *105*, 6826–6833.

- (32) Zhang, Y.; Cremer, P. S. Chemistry of Hofmeister Anions and Osmolytes. *Annu. Rev. Phys. Chem.* **2010**, *61*, 63–83.
- (33) McAfee, M. S.; Zhang, H.; Annunziata, O. Amplification of salt-induced polymer diffusiophoresis by increasing salting-out strength. *Langmuir* **2014**, *30*, 12210–12219.
- (34) Timasheff, S. N. Protein-solvent preferential interactions, protein hydration, and the modulation of biochemical reactions by solvent components. *Proc. Natl. Acad. Sci. U. S. A.* **2002**, *99*, 9721–9726.
- (35) Pusey, P. N.; van Megen, W. Phase behaviour of concentrated suspensions of nearly hard colloidal spheres. *Nature* **1986**, *320*, 340–342.
- (36) Broide, M. L.; Berland, C. R.; Pande, J.; Ogun, O.; Benedek, G. B. Binary-liquid phase separation of lens protein solutions. *Proc. Natl. Acad. Sci. U. S. A.* **1991**, *88*, 5660–5664.
- (37) Record, M. T.; Anderson, C. F. Interpretation of preferential interaction coefficients of nonelectrolytes and of electrolyte ions in terms of a two-domain model. *Biophys. J.* **1995**, *68*, 786–794.
- (38) Lekkerkerker, H. N. W.; Poon, W. C. K.; Pusey, P. N.; Stroobants, A.; Warren, P. B. Phase Behaviour of Colloid + Polymer Mixtures. *Europhys. Lett.* **1992**, *20*, 559–564.
- (39) Niu, Y.; Sun, L.; Crooks, M. Determination of the Intrinsic Proton Binding Constants for Poly(amidoamine) Dendrimers via Potentiometric pH Titration. *Macromolecules* **2003**, *36*, 5725–5731.
- (40) Carnahan, N. F.; Starling, K. E. Equation of state for nonattracting rigid spheres. *J. Chem. Phys.* **1969**, *51*, 635–636.
- (41) Hansen, J.-P.; McDonald, I. R. *Theory of simple liquids*, 4th ed.; Academic Press: Oxford, 2013.
- (42) Mansoori, G. A.; Carnahan, N. F.; Starling, K. E.; Leland, T. W., Jr. Equilibrium thermodynamic properties of the mixture of hard spheres. *J. Chem. Phys.* **1971**, *54*, 1523–1525.
- (43) Amokrane, S.; Regnaut, C. Free-volume fraction in hard-sphere mixtures and the osmotic spinodal curve. *Phys. Rev. E: Stat. Phys., Plasmas, Fluids, Relat. Interdiscip. Top.* **1996**, *53*, 1990–1993.
- (44) Rard, J. A.; Clegg, S. L.; Palmer, D. A. Isopiestic Determination of the Osmotic Coefficients of Na₂SO₄(aq) at 25 and 50°C, and Representation with Ion-Interaction (Pitzer) and Mole Fraction Thermodynamic Models. *J. Solution Chem.* **2000**, *29*, 1–49.
- (45) Yethiraj, A.; Hall, C. K. Generalized Flory equations of state for square-well chains. *J. Chem. Phys.* **1991**, *95*, 8494–8506.
- (46) Wertheim, M. S. Fluids of dimerizing hard spheres, and fluid mixtures of hard spheres and dispheres. *J. Chem. Phys.* **1986**, *85*, 2929–2936.
- (47) Annunziata, O.; Pande, A.; Pande, J.; Ogun, O.; Lubsen, N. H.; Benedek, G. B. Oligomerization and phase transitions in aqueous solutions of native and truncated human beta B1-crystalline. *Biochemistry* **2005**, *44*, 1316–1328.
- (48) Asherie, N.; Pande, J.; Lomakin, A.; Ogun, O.; Hanson, S. R. A.; Smith, J. B.; Benedek, G. B. Oligomerization and phase separation in globular protein solutions. *Biophys. Chem.* **1998**, *75*, 213–227.
- (49) Zhang, F.; Roth, R.; Wolf, M.; et al. Charge-controlled metastable liquid–liquid phase separation in protein solutions as a universal pathway towards crystallization. *Soft Matter* **2012**, *8*, 1313–1316.
- (50) Matsarskaia, O.; Braun, M. K.; Roosen-Runge, F.; et al. Cation-Induced Hydration Effects Cause Lower Critical Solution Temperature Behavior in Protein Solutions. *J. Phys. Chem. B* **2016**, *120*, 7731–7736.
- (51) Roosen-Runge, F.; Zhang, F.; Schreiber, F.; Roth, R. Ion-activated attractive patches as a mechanism for controlled protein interactions. *Sci. Rep.* **2015**, *4*, 7016.